

STRENGTH OF MATERIALS UNDER STATIC LOADING IN THE DIAMOND ANVIL CELL

T. S. Duffy¹

¹*Department of Geosciences, Princeton University, Princeton, NJ 08544*

Abstract. Strength properties of materials under static and dynamic loading are essential quantities for characterizing mechanical behavior. Quantitative measurements of static strengths achieved in the diamond anvil cell can be made using x-ray diffraction in a radial geometry for samples under non-hydrostatic compression. Results for several metals up to 68 GPa show that the ratio of yield strength to shear modulus ranges from 0.01-0.03 and increases weakly with compression. Trends at lower pressure for Re, W, and ϵ -Fe are consistent with available data above 1 Mbar. Strong ceramics such as B_6O , $c\text{-Si}_3\text{N}_4$, and TiB_2 achieve yield strengths as large as 10% of the shear modulus at pressures up to ~ 70 GPa. Strengths of materials used as pressure media are quantitatively compared and evaluated.

Keywords: yield strength, x-ray diffraction, high pressure, metals.

PACS: 62.50.+p, 62.20.Fe, 61.10.-i.

INTRODUCTION

Mechanical properties and strength at ultrahigh pressures have been of interest since the advent of high-pressure techniques [1]. Applications include optimizing the design and performance of static high-pressure apparatus and improving ballistics performance under dynamic loading. Basic questions regarding strength include how pressure affects yield strength and how the strengths of different classes of materials compare at ultrahigh pressures [2]. Development of new methods for dynamic loading under shock and quasi-isentropic conditions has also spurred renewed interest in material strength [3,4].

In the diamond anvil cell, qualitative methods to identify non-hydrostatic stresses were developed from observation of pressure gradients and linewidths of ruby fluorescence peaks. Quantitative measurements of shear strength followed from considering the balance between the radial pressure gradient and the shear stress at the

anvil-sample interface which yields the relation [5] (Fig. 1):

$$\tau = \frac{h}{2} \frac{dP}{dr}, \quad (1)$$

where τ is the shear stress, dP/dr is the radial pressure gradient, usually obtained from ruby fluorescence measurements, and h is the sample thickness. A second method for stress determination uses measurements of the ellipticity of diffraction rings formed by x-rays which pass perpendicularly to the axis of the diamond cell [6]. Renewed development of this radial diffraction method [7] in recent years has led to rapid growth in characterization of strength effects at high pressures as well as opportunities for studying elasticity, equations of state, and deformation mechanisms at extreme conditions.

THEORY

In radial x-ray diffraction experiments, a sample is compressed under intentionally non-hydrostatic conditions and the elastic lattice strain is measured as a function of the angle from the loading axis using synchrotron x-rays (e.g. [7,8]) (Fig. 1). The stress state in a polycrystalline sample under uniaxial compression in the diamond anvil cell is described by a maximum stress along the cell loading axis, σ_3 , and a minimum stress in the radial direction, σ_1 . The difference between σ_3 and σ_1 is the differential stress, t :

$$t = \sigma_3 - \sigma_1 \leq 2\tau = Y, \quad (2)$$

where Y the yield strength of the sample. The equality in Eqn. (2) holds for a Von Mises yield condition and t could be less than the yield strength.

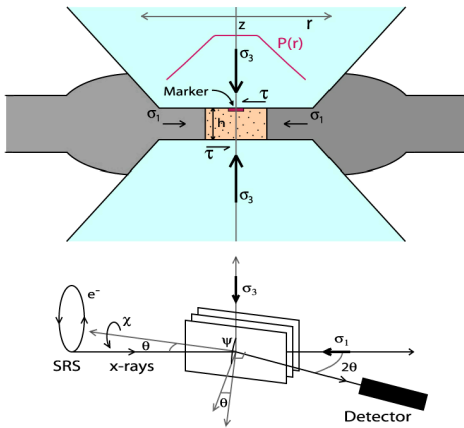


Figure 1. Schematic illustration of diffraction geometry in a radial x-ray experiment in the diamond cell with ED detector. r , z are the radial and axial coordinates, respectively, χ is the cell rotation angle, $P(r)$ is the radial pressure distribution, and θ is the diffraction angle.

The observed d -spacings (d_m) for a set of planes (hkl) measured by x-ray diffraction are a function of the angle ψ between the diamond cell axis and normal to the diffraction planes (Figs. 1 and 2):

$$d_m(hkl) = d_p(hkl)[1 + (1 - 3\cos^2\psi)Q(hkl)], \quad (3)$$

where $d_p(hkl)$ is the d spacing resulting from the hydrostatic component of stress, and $Q(hkl)$ is given by:

$$Q(hkl) = \frac{t}{3} \left\{ \frac{\alpha}{2G_R(hkl)} + \frac{(1 - \alpha)}{2G_V} \right\}. \quad (4)$$

$G_R(hkl)$ is the aggregate shear modulus of grains contributing to the diffraction intensity under the condition of constant stress across grain boundaries (Reuss limit). G_V is the shear modulus under isostrain conditions (Voigt bound).

According to Eqn. (3), $d_m(hkl)$ should vary linearly with $1-3\cos^2\psi$ (Fig. 2). At $\psi = 54.7^\circ$ ($1-3\cos^2\psi = 0$), the position of the observed x-ray diffraction line reflects the d spacing due to the hydrostatic component of stress only.

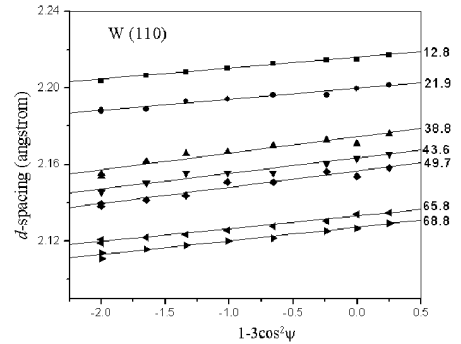


Figure 2. Variation in d -spacing with angle from load axis for the (110) diffraction peak of tungsten [9]. Pressures in GPa are indicated on the right.

The aggregate polycrystalline sample in the diamond anvil cell is generally assumed to be under isostress conditions. In this case, α is equal to 1 in Eqn. (4) and the differential stress can be expressed as:

$$t = 6G_R <Q(hkl)>, \quad (5)$$

where $<Q(hkl)>$ represents the average $Q(hkl)$ value over all observed reflections, and G_R is the Reuss bound on the aggregate shear modulus of the polycrystalline sample. If the differential stress, t , has reached its limiting value of the yield strength

at high pressures, $6\langle Q(hkl)\rangle = t/G$, will reflect the ratio of yield strength to shear modulus. Orientation dependence of strength may be important in detail, but here we focus solely on mean strength.

Microscopic deviatoric stress also exists in a polycrystalline sample under compression as a result of grain-to-grain contact and/or strength of the pressure medium. This stress field leads to broadening of x-ray diffraction peaks. Experimental studies in both large-volume apparatus and the diamond cell have also used measurements of broadening to constrain strength from the microscopic stress distribution [9-11].

EXPERIMENTAL METHODS

Upon loading in the diamond anvil cell, an equilibrium pressure gradient is established (Fig. 1). The stress distribution is assumed to be radially symmetric about the load axis and the axial stress gradient is negligible [12]. In the earliest stages of compression, the sample undergoes compaction, followed by elastic and then plastic deformation. The sample can undergo considerable plastic deformation even at low pressures. Strain rates are not directly measured but are low ($<10^{-1} \text{ s}^{-1}$). Grain size may also decrease with compression.

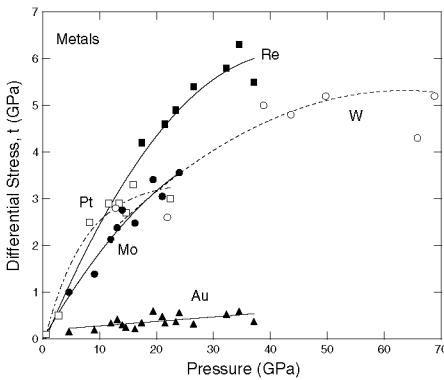


Figure 3. Differential stress as a function of pressure from radial x-ray diffraction data for the metals Re W, Mo, Pt, and Au. Experimental results are from [8,9,13,14].

In the radial x-ray diffraction geometry, the sample is confined by a gasket made of Be or other

x-ray transparent material. Incident and diffracted synchrotron x-rays pass through the gasket and the d spacing and intensity of individual diffraction lines are determined as a function of the angle from the loading axis, ψ [7] (Fig. 1). A small piece of a standard is placed at the center of the sample to serve as a positional reference and pressure marker. Experiments can be performed in energy-dispersive (ED) or angle-dispersive (AD) geometry. The advantage of the ED geometry [8] is that spatial filtering allows restriction of diffraction signal to the central part of the sample where the lattice strain equations strictly apply. However, this method has both lower resolution (in d spacing) and is more time consuming. The AD geometry [15], on the other hand, is considerably faster allowing for simultaneous accumulation of the full Debye-Scherrer ellipses but it does not readily allow for spatial filtering.

RESULTS AND DISCUSSION

Figure 3 shows differential stresses measured for several metals using the ED radial diffraction technique. For most materials, the differential stress increases with compression and eventually flattens out somewhat at higher pressures (cf. Fig. 6). This flattening suggests yielding is occurring and supports identification of t with the yield strength under these loading conditions.

Rhenium, which has the largest shear modulus of any metal, supports the highest differential stresses (up to 6.3 GPa at a pressure of 37 GPa). W and Mo are bcc metals with moderately high shear moduli. Both support comparable differential stresses up to 25 GPa (Fig. 3) and t values up to 5.2 GPa have been measured for W at 68 GPa [9]. The yield strength of W has also been measured under shock and quasi-isentropic loading [16]. The static strength is much larger than strengths along the Hugoniot but very similar to values observed under quasi-isentropic loading despite large differences in strain rates [9].

Gold is a noble metal with an fcc structure that is widely used as a pressure calibrant in static high-pressure studies. From 8 to 37 GPa, the differential stress of gold can be described by the following relation [8,13]:

$$t \text{ (GPa)} = 0.18 + 0.01P \text{ (GPa)}. \quad (6)$$

At 37 GPa, the strength of gold is just 0.4-0.6 GPa, significantly below other metals examined. The predicted strength at 1 Mbar from Eqn. (6) is about 1.2 GPa. Platinum is also widely used as a pressure calibrant and laser absorber in the diamond anvil cell. Despite a relatively low shear modulus ($G=61$ GPa), Pt appears to support relatively large differential stresses [14] (Fig. 3).

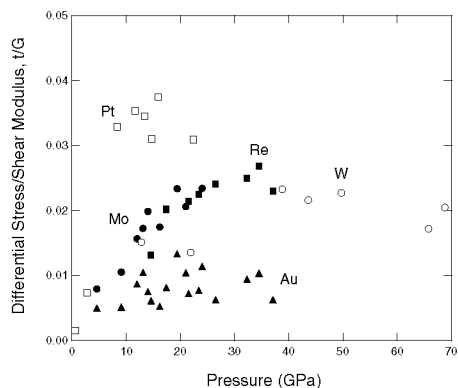


Figure 4. Ratio of differential stress to shear modulus as a function of pressure for selected metals.

Figure 4 shows the ratio of differential stress to shear modulus for the metals studied here. This quantity is determined directly from the mean slope of the d spacing- ψ relation (Eqns. 3 and 5). The incompressible metals (Re, W, Mo) exhibit differential stresses that are about 2-3% of the shear modulus under these loading conditions. Furthermore, t/G tends to increase weakly with pressure. That is, the differential stress increases at a faster rate than the shear modulus. This likely reflects the contributions of both pressure and strain hardening to the measured yield strength.

In the case of Au, the t/G values are less than 0.01 up to 37 GPa. Pt, on the other hand, exhibits t values that exceed 3% of the shear modulus. In view of its importance, further studies on Pt are warranted to confirm these observations and extend them to higher pressures.

Measurements of static strength at pressures above 1 Mbar are limited at present (Fig. 5). Measurements of diffraction of ϵ -Fe and W at $\psi = 0^\circ$ and 90° were carried out to pressures as high as

300 GPa [17]. In another study, the yield strength of Re at 100 GPa was estimated from comparison of finite element models with experimental gasket thicknesses [18]. Differential stresses have been measured in (Mg,Fe)SiO₃ and MgGeO₃ post-perovskites (CaIrO₃-type) using radial diffraction techniques [15,19] at 104-157 GPa, although these values are probably lower bounds to the yield strength because the samples were laser heated and this would be expected to partially release differential stresses.

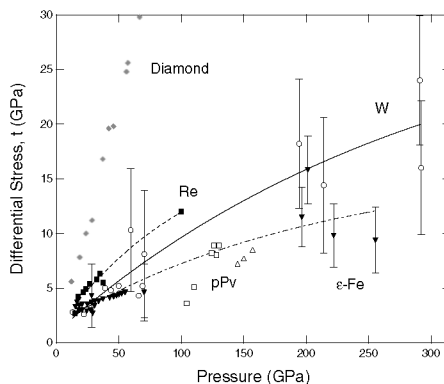


Figure 5. Summary of differential stress measurements at pressures above 1 Mbar. Lines are fits that connect low-pressure and high-pressure measurements. pPv – germanates and silicates in the post-perovskite structure. Experimental results are from [8,9,11,15,17-21].

In Fig. 5, measurements [17,18] at $P > 1$ Mbar for W, ϵ -Fe, and Re are compared with lower pressure studies [8,9,11,21]. The high-pressure data are broadly consistent with trends observed at lower pressures (e.g., $t_{Re} > t_W > t_{\epsilon-Fe}$). Yield strength continues to increase to Mbar pressures such that for ϵ -Fe and W differential stresses at ultrahigh pressures are about 2-5 times larger than observed for these metals near 50 GPa. For W, t values at 300 GPa are ~3-5% of the expected shear modulus at this pressure, suggesting that t/G continues to increase with compression to ultrahigh pressures. Moreover, the t values measured at these extreme conditions may be a lower bound to the yield strength as anvil deformation may limit development of differential stresses [17].

Radial x-ray diffraction experiments have also been carried out up to 68 GPa on a variety of strong ceramics including B_2O_3 [22], Si_3N_4 (spinel structure) [23], TiB_2 [24] and silicates such as ringwoodite [25], stishovite [26], and perovskite [27] (Fig. 6). Differential stresses in these ceramics greatly exceed those observed in metals. The strongest materials measured to date include B_2O_3 and TiB_2 which sustain differential stresses near 28-30 GPa at mean pressures of 60-65 GPa. For comparison, the differential stress in TiB_2 was determined to be 42 GPa at 61 GPa along the Hugoniot [28]. The values of t/G for these materials increase under static loading and differential stresses reach 8-10% of the shear modulus at the highest pressures for B_2O_3 and cubic Si_3N_4 , considerably greater than values observed for metals.

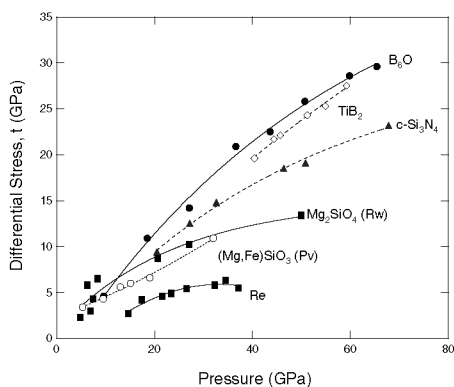


Figure 6. Differential stresses in selected strong ceramics including oxides, borides, nitrides, and silicates. t values for Re metal are shown for comparison. Rw—ringwoodite; Pv- perovskite; c- Si_3N_4 —cubic (spinel-type) silicon nitride. Data are from [22-25,27].

Hydrostatic pressure conditions are optimum for many types of high-pressure experiments but are difficult to achieve at room temperature. A variety of soft pressure transmitting media have been employed to achieve quasi-hydrostatic conditions in diamond cell experiments. In laser heating experiments, an insulating medium is needed to reduce axial temperature gradients [29]. While qualitative constraints on relative strengths of various pressure and insulating media have long

been known, the radial x-ray diffraction method now allows quantitative limits to be placed on the maximum differential stresses that may be sustained. Results for several materials used as pressure media are summarized in Fig. 7. MgO is relatively strong but there are large differences in strengths reported in diamond anvil [30] and large-volume press experiments [31]. These stress differences may be related to higher levels of plastic strain achieved in the DAC experiments [31]. In addition, the evolution of grain size with pressure may play a role [32].

Limited data on NaCl suggests that it supports relatively small differential stresses (0.5-0.8 GPa at 19 GPa confining pressure) [33]. At modest pressures, solid argon has the lowest observed t value (0.4 GPa at 28 GPa pressure), although there is evidence that the strength of Ar begins to increase rapidly above 30 GPa [34]. While CaO is not commonly considered as a pressure medium, it is notable that at 40 GPa and above, differential stresses in CaO are actually lower than those in Ar [35]. This shows how quantitative measurements of differential stresses are valuable for characterizing material behavior and identifying candidates for insulating and pressure transmitting media over different ranges of compression.

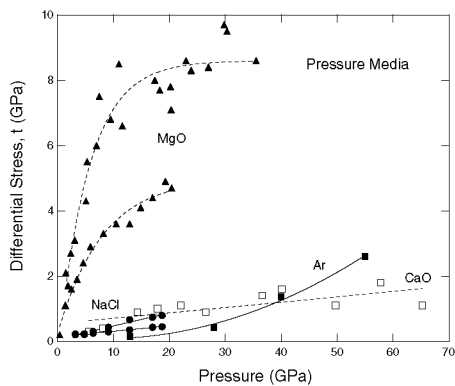


Figure 7. Differential stresses in materials commonly used as pressure transmitting or insulation media in diamond anvil cell experiments. Refs: MgO [30,31], NaCl [33], Ar [34], CaO [35].

CONCLUSIONS

In general, strength increases with compression at a rate greater than the shear modulus, implying significant strain hardening under diamond cell loading conditions. At pressures of 20-80 GPa, metals typically exhibit strengths of 1-3% of the shear modulus, G . Strong covalent oxides, silicates, and nitrides such as ringwoodite, boron suboxide, and spinel-structured silicon nitride possess yield strengths that can approach 10% of the shear modulus. The maximum strength value we have measured is 28 GPa for B_6O at 65 GPa confining pressure. The general increase in strength with pressure for all material classes implies that most materials are "strong" at Mbar pressures if one recognizes that the strength of high-grade steel at ambient pressure is ~ 2 GPa. Furthermore, the consistency of general strength trends across material classes suggests that reasonable empirical predictions of strength in the multi-Mbar pressure regime can now be made.

ACKNOWLEDGEMENTS

Funding was provided by the NSF and the Carnegie-DOE Alliance Center. S. Dorfman provided assistance in figure preparation.

REFERENCES

1. Bridgman, P. W., *Physical Review* 48, 825 (1935).
2. Brazhkin, V. V. and Lyapin, A. G., *Journal of Physics-Condensed Matter* 14, 10861 (2002).
3. Vogler, T. J. and Chhabildas, L. C., *International Journal of Impact Engineering* 33, 812 (2006).
4. Smith, R. F., Eggert, J. H., Jankowski, A. et al., *Physical Review Letters* 98, 065701 (2007).
5. Sung, C. M., Goetze, C., and Mao, H.-k., *Review of Scientific Instruments* 48, 1386 (1977).
6. Singh, A. K. and Kennedy, G. C., *Journal of Applied Physics* 45, 4686 (1974).
7. Singh, A. K., Balasingh, C., Mao, H.-k. et al., *Journal of Applied Physics* 83, 7567 (1998).
8. Duffy, T. S., Shen, G., Heinz, D. L. et al., *Physical Review B* 60, 15063 (1999).
9. He, D. and Duffy, T. S., *Physical Review B* 73, 134106 (2006).
10. Weidner, D. J., Wang, Y. B., and Vaughan, M. T., *Geophysical Research Letters* 21, 753 (1994).
11. Singh, A. K., Jain, A., Liermann, H. P. et al., *Journal of Physics and Chemistry of Solids* 67, 2197 (2006).
12. Merkel, S., *Journal of Physics - Condensed Matter* 18, S949 (2006).
13. Duffy, T. S., Shen, G., Shu, J. F. et al., *Journal of Applied Physics* 86, 6729 (1999).
14. Kavner, A. and Duffy, T. S., *Physical Review B* 68, 144101 (2003).
15. Merkel, S., McNamara, A. K., Kubo, A. et al., *Science* 316, 1729 (2007).
16. Chhabildas, L. C., Asay, J. R., and Barker, L. M., SNL Report No. SAND88-0306.UC-34, 1988.
17. Hemley, R. J., Mao, H.-k., Shen, G. et al., *Science* 276, 1242 (1997).
18. Merkel, S., Hemley, R. J., and Mao, H.-k., *Applied Physics Letters* 74, 656 (1999).
19. Merkel, S., Kubo, A., Miyagi, L. et al., *Science* 311, 644 (2006).
20. Akahama, Y. and Kawamura, H., *Journal of Applied Physics* 98, 083523 (2005).
21. Merkel, S., Shu, J. F., Gillet, P. et al., *Journal of Geophysical Research* 110 (2005).
22. He, D., Shieh, S. R., and Duffy, T. S., *Physical Review B* 70, 184121 (2004).
23. Kiefer, B., Shieh, S. R., Duffy, T. S. et al., *Physical Review B* 72, 014102 (2005).
24. Amulele, G. M., Manghnani, M. H., and Somayazulu, M., *Journal of Applied Physics* 99, 023522 (2006).
25. Kavner, A. and Duffy, T. S., *Geophysical Research Letters* 28, 2691 (2001).
26. Shieh, S. R., Duffy, T. S., and Li, B. S., *Physical Review Letters* 89, 25507 (2002).
27. Merkel, S., Wenk, H. R., Badro, J. et al., *Earth and Planetary Science Letters* 209, 351 (2003).
28. Dandekar, D. P. and Benfanti, D. C., *Journal of Applied Physics* 73, 673 (1993).
29. Kiefer, B. and Duffy, T. S., *Journal of Applied Physics* 97, 114902 (2005).
30. Merkel, S., Wenk, H. R., Shu, J. F. et al., *Journal of Geophysical Research* 107, 2271 (2002).
31. Uchida, T., Wang, Y. B., Rivers, M. L. et al., *Earth and Planetary Science Letters* 226, 117 (2004).
32. Singh, A. K., Liermann, H. P., and Saxena, S. K., *Solid State Communications* 132, 795 (2004).
33. Funamori, N., Yagi, T., and Uchida, T., *Journal of Applied Physics* 75, 4327 (1994).
34. Mao, H.-k., Badro, J., Shu, J. F. et al., *Journal of Physics-Condensed Matter* 18, S963 (2006).
35. Speziale, S., Shieh, S. R., and Duffy, T. S., *Journal of Geophysical Research* 111, B02203 (2006).